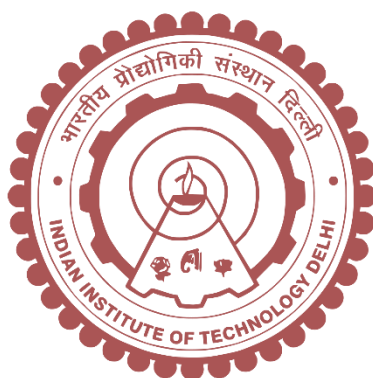


**FROM SEQUENCE TO STRUCTURE:
HIERARCHICAL SELF-ASSEMBLY INTO
STRUCTURALLY DISTINCT ARCHITECTURES**

SOUVIK DUTTA



**DEPARTMENT OF CHEMISTRY
INDIAN INSTITUTE OF TECHNOLOGY DELHI
JANUARY 2026**

©Indian Institute of Technology Delhi (IITD), New Delhi, 2026

**FROM SEQUENCE TO STRUCTURE:
HIERARCHICAL SELF-ASSEMBLY INTO
STRUCTURALLY DISTINCT ARCHITECTURES**

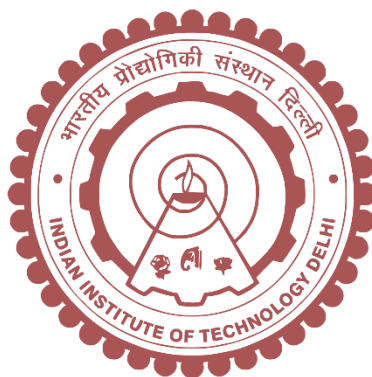
by

SOUVIK DUTTA

(Entry No. 2021CZY8386)

Submitted

in fulfilment of the requirements of the degree of Doctor of Philosophy
to the



Indian Institute of Technology Delhi

Hauz Khas, New Delhi, India-110016

January 2026

DEDICATED TO
MY PARENTS AND MY SISTER

CERTIFICATE

This is to certify that the thesis, entitled "**From Sequence to Structure: Hierarchical Self-Assembly into Structurally Distinct Architectures**", being submitted by **Mr. Souvik Dutta**, to the Indian Institute of Technology Delhi, for the award of degree of **Doctor of Philosophy** in Chemistry, is a record of bonafide research work carried out by him. **Mr. Souvik Dutta** has worked under my guidance and supervision and has fulfilled all the requirements for the submission of this thesis, which to my knowledge has reached the requisite standard. The results embodied in this thesis have not been submitted in part or in full, to any other University or Institute for award of any degree or diploma.

Prof. V. Haridas

Professor

Department of Chemistry

Indian Institute of Technology Delhi

Hauz Khas, New Delhi-110016, India.

ACKNOWLEDGEMENTS

It is with great pleasure and deep respect that I express my profound gratitude to my supervisor, **Prof. V. Haridas**, for his invaluable guidance, encouragement, and unwavering support throughout the course of my doctoral research. His scientific ideas, insightful discussions, and constant motivation have been instrumental in shaping my research ideas and nurturing my overall growth as a researcher. His patience, generosity with time, and high standards of academic rigor have greatly inspired me and will continue to influence my future endeavours. I feel extremely fortunate for having the opportunity to work under his supervision.

I am also sincerely thankful to the members of my Student Research Committee (SRC), **Prof. Nalin Pant, Prof. Janakiram Vaitla** and **Prof. Bishwajit Kundu**, for their valuable feedback, constructive criticism, and kind encouragement during the course of my research. Their suggestions not only helped me refine my work but also gave me new perspectives to pursue challenging problems with confidence.

I extend my heartfelt thanks to the **Indian Institute of Technology Delhi, Hauz Khas, New Delhi**, for providing me with the opportunity to pursue my doctoral studies in such a vibrant academic environment and for my fellowship. I am grateful to the **past and present Heads of the Department of Chemistry, Prof. A. J. Elias, Prof. S. Pandey** and **Prof. S. Nagendran**, for their constant support in building and maintaining a stimulating and resourceful research atmosphere within the department.

I also take this opportunity to thank all the **faculty members of the Department of Chemistry, IIT Delhi**, for their inspiring lectures, critical discussions, and encouragement during my academic journey. I am equally indebted to all the **staff members of the department**, whose help and cooperation have been indispensable in the smooth functioning of both academic and research activities.

I gratefully acknowledge the use of **CRF and SATHI facilities at IIT Delhi**, which provided access to instrumentation and resources essential for the successful completion of my research work.

I owe a special note of thanks to all my **past and present lab members**, whose scientific discussions, and collaborative spirit made the lab a lively and motivating place to work in. Their companionship has been a source of both professional learning and personal joy.

Finally, I express my deepest gratitude to my **parents, sister and friends**, whose unconditional love, encouragement, and sacrifices have been my greatest strength throughout my life. Their constant support during difficult times and belief in my abilities gave me the confidence to overcome challenges and persevere in my work. This thesis is as much their achievement as it is mine, and I dedicate this accomplishment to them with immense affection and respect.

January 2026

Souvik Dutta .

Souvik Dutta

ABSTRACT

This thesis, entitled "**From Sequence to Structure: Hierarchical Self-Assembly into Structurally Distinct Architectures**", explores the design, synthesis, and self-assembly behaviour of pseudopeptides functionalized with phenylene urea motifs, demonstrating how subtle changes in molecular architecture and amino acid sequence can lead to diverse supramolecular structures. Through a combination of spectroscopic, crystallographic, and microscopic techniques, we investigate the role of non-covalent interactions, such as π - π stacking, hydrogen bonding, and hydrophobic clustering, in directing the formation of nanotubes, fibers, vesicles, toroids, and zipper-like assemblies. The autofluorescent properties of these assemblies further enhance their potential for bioimaging applications. Overall, this work highlights the versatility of urea-based scaffolds in mimicking biological folding and in forming complex architectures with the help of self-assembly.

Chapter 1

Chapter 1 provides a comprehensive introduction to self-assembly in biological systems, emphasizing the fundamental principles and significance of this phenomenon in nature. It discusses how weak, non-covalent interactions, including hydrogen bonds, hydrophobic interactions, and electrostatic forces, drive the ordered organization of molecules into functional structures such as proteins, membranes, and DNA. The chapter highlights the central role of peptides as minimal, versatile building blocks for creating a wide array of nanostructures like fibers, nanotubes, and vesicles, outlining the advantages of synthetic peptides over natural proteins. Additionally, it states the diverse applications of self-assembled peptides and pseudopeptides in areas such as drug delivery, tissue engineering, biosensing, catalysis, nanoelectronics, and antimicrobial therapies, while addressing current challenges and future research directions in the field.

Chapter 2

Chapter 2 introduces a novel peptide design strategy where a phenylene urea aglet at the N-terminus induces a reverse turn conformation via edge-to-face π - π interactions. This leads to the formation of polygonal peptide tubes through a Phe-zipper arrangement, as confirmed by X-ray crystallography and electron microscopy. Single-crystal X-ray diffraction analysis

reveals that one of the derivatives adopts a left-handed triple-helical conformation, stabilized through a combination of intermolecular hydrogen bonding and hydrophobic interactions.

Chapter 3

Chapter 3 extends the design to include aliphatic residues (Leu/Ile) alongside Phe, resulting in tubular assemblies via Leu/Ile-Phe zipper motifs. Single-crystal X-ray analysis reveals a double-helical arrangement stabilized by intermolecular hydrogen bonds and hydrophobic interactions. The resulting nanostructures exhibit concentration-dependent autofluorescence and red-edge excitation shift (REES), enabling confocal imaging of the self-assembled architectures.

Chapter 4

Chapter 4 investigates the concentration-dependent morphological evolution of urea-cored pseudopeptides, which transition from vesicles to toroids and eventually to multi-torus and honeycomb-like structures. This study provides insights into the fusion mechanisms of synthetic peptide-based vesicles and highlights the influence of sequence and concentration on supramolecular topology. The autofluorescence of these structures is morphology-dependent, allowing optical visualization of assembly pathways.

Chapter 5

Chapter 5 demonstrates the use of phenyl urea as an aglet to stabilize the trans conformation of prolyl peptide bonds via $n \rightarrow \pi^*$ interactions. X-ray crystallography confirms the exclusive trans geometry and reveals an Ile-Phe zipper-like clustering of hydrophobic side chains in non-aqueous media. This chapter underscores the ability of urea tags to control peptide conformation and promote biomimetic hydrophobic assembly even in organic solvents.

सारांश

"अनुक्रम से संरचना तक: संरचनात्मक रूप से विशिष्ट संरचनाओं में पदानुक्रमित स्व-संयोजन" शीर्षक वाला यह शोध प्रबंध, फ़िनिलीन यूरिया रूपांकनों से क्रियाशील स्यूडोपेप्टाइड्स के डिज़ाइन, संश्लेषण और स्व-संयोजन व्यवहार का अन्वेषण करता है, यह दर्शाता है कि आणविक संरचना और अमीनो अम्ल अनुक्रम में सूक्ष्म परिवर्तन कैसे विविध अतिआणविक संरचनाओं को जन्म दे सकते हैं। स्पेक्ट्रोस्कोपिक, क्रिस्टलोग्राफिक और सूक्ष्म तकनीकों के संयोजन के माध्यम से, हम नैनोट्यूब, रेशों, पुटिकाओं, टोरॉइड और ज़िपर जैसी संरचनाओं के निर्माण को निर्देशित करने में गैर-सहसंयोजक अंतःक्रियाओं—जैसे $\pi-\pi$ स्टैकिंग, हाइड्रोजन बॉन्डिंग और हाइड्रोफोबिक क्लस्टरिंग—की भूमिका की जाँच करते हैं। इन संरचनाओं के स्व-प्रतिदीप्ति गुण जैव-चित्रण अनुप्रयोगों के लिए उनकी क्षमता को और बढ़ाते हैं। कुल मिलाकर, यह कार्य जटिल जैविक वलन और संयोजन परिघटनाओं की नकल करने में यूरिया-आधारित मचानों की बहुमुखी प्रतिभा को उजागर करता है।

अध्याय 1

अध्याय 1 जैविक प्रणालियों में स्व-संयोजन का एक व्यापक परिचय प्रदान करता है, और प्रकृति में इस परिघटना के मूलभूत सिद्धांतों और महत्व पर बल देता है। यह चर्चा करता है कि कैसे हाइड्रोजन बंध, जलभीतिक अंतःक्रियाएँ और स्थिरवैद्युत बल सहित दुर्बल, असहसंयोजक अंतःक्रियाएँ अणुओं को प्रोटीन, झिल्लियों और डीएनए जैसी कार्यात्मक संरचनाओं में व्यवस्थित रूप से व्यवस्थित करती हैं। यह अध्याय रेशों, नैनोट्यूब और पुटिकाओं जैसी नैनो संरचनाओं की एक विस्तृत श्रृंखला के निर्माण के लिए न्यूनतम, बहुमुखी निर्माण खंडों के रूप में पेप्टाइड्स की केंद्रीय भूमिका पर प्रकाश डालता है, और प्राकृतिक प्रोटीन की तुलना में सिंथेटिक पेप्टाइड्स के लाभों को रेखांकित करता है। इसके अतिरिक्त, यह औषधि वितरण, ऊतक अभियांत्रिकी, जैवसंवेदन, उत्प्रेरण, नैनोइलेक्ट्रॉनिक्स और रोगाणुरोधी चिकित्सा जैसे क्षेत्रों में स्व-संयोजन पेप्टाइड्स और स्यूडोपेप्टाइड्स के विविध अनुप्रयोगों को बताता है, साथ ही इस क्षेत्र में वर्तमान चुनौतियों और भविष्य की अनुसंधान दिशाओं पर भी प्रकाश डालता है।

अध्याय 2

अध्याय 2 एक नवीन पेप्टाइड डिज़ाइन रणनीति प्रस्तुत करता है जहाँ N-टर्मिनस पर एक फेनिलीन यूरिया एग्लेट, किनारे-से-सामने $\pi-\pi$ अंतःक्रियाओं के माध्यम से एक विपरीत मोड़ संरचना उत्पन्न करता है। इससे Phe-ज़िपर व्यवस्था के माध्यम से बहुभुज पेप्टाइड नलिकाओं का निर्माण होता है, जैसा कि एक्स-

रे क्रिस्टलोग्राफी और इलेक्ट्रॉन माइक्रोस्कोपी द्वारा पुष्टि की गई है। एकल-क्रिस्टल एक्स-रे विवर्तन विश्लेषण से पता चलता है कि व्युत्पन्न में से एक, अंतर-आणविक हाइड्रोजन बंधन और हाइड्रोफोबिक अंतःक्रियाओं के संयोजन द्वारा स्थिर, एक बाएँ-हस्त त्रि-हेलिकल संरचना को अपनाता है।

अध्याय 3

अध्याय 3 डिज़ाइन का विस्तार करते हुए Phe के साथ-साथ एलिफैटिक अवशेषों (Leu/Ile) को शामिल करता है, जिसके परिणामस्वरूप Leu/Ile-Phe ज़िपर रूपांकनों के माध्यम से नलिकाकार संयोजन बनते हैं। एकल-क्रिस्टल एक्स-रे विश्लेषण से अंतर-आणविक हाइड्रोजन बंधों और हाइड्रोफोबिक अंतःक्रियाओं द्वारा स्थिर एक द्वि-हेलिकल व्यवस्था का पता चलता है। परिणामी नैनो संरचनाएँ सांद्रता-निर्भर स्वप्रतिदीप्ति और लाल-किनारा उत्तेजन विस्थापन (REES) प्रदर्शित करती हैं, जिससे स्व-संयोजित संरचनाओं की कॉन्फोकल इमेजिंग संभव होती है।

अध्याय 4

अध्याय 4 यूरिया-कोरयुक्त स्यूडोपेप्टाइड्स के सांद्रता-निर्भर रूपात्मक विकास की जाँच करता है, जो पुटिकाओं से टोरॉइड और अंततः बहु-टोरस और छत्ते जैसी संरचनाओं में परिवर्तित होते हैं। यह अध्ययन सिंथेटिक पेप्टाइड-आधारित पुटिकाओं के संलयन तंत्रों में अंतर्दृष्टि प्रदान करता है और सुपरमॉलेक्यूलर टोपोलॉजी पर अनुक्रम और सांद्रता के प्रभाव पर प्रकाश डालता है। इन संरचनाओं का स्वप्रतिदीप्ति आकारिकी-निर्भर है, जिससे संयोजन पथों का प्रकाशीय दृश्यीकरण संभव होता है।

अध्याय 5

अध्याय 5 $n \rightarrow \pi^*$ अंतःक्रियाओं के माध्यम से प्रोलिल पेप्टाइड बंधों के ट्रांस संरूपण को स्थिर करने के लिए एग्लेट के रूप में फेनिल यूरिया के उपयोग को प्रदर्शित करता है। एक्स-रे क्रिस्टलोग्राफी विशिष्ट ट्रांस ज्यामिति की पुष्टि करती है और गैर-जलीय माध्यम में हाइड्रोफोबिक पार्श्व श्रृंखलाओं के इले-फे ज़िपर जैसे समूहन को प्रकट करती है। यह अध्याय यूरिया टैग्स की पेप्टाइड संरचना को नियंत्रित करने और कार्बनिक विलायकों में भी बायोमिमेटिक हाइड्रोफोबिक संयोजन को बढ़ावा देने की क्षमता को रेखांकित करता है।

ENCLOSURES

CERTIFICATE.....	i
ACKNOWLEDGEMENTS.....	ii
ABSTRACT.....	iv
TABLE OF CONTENTS.....	ix
LIST OF FIGURES.....	xiii
LIST OF TABLES.....	xxv
LIST OF SCHEMES.....	xxvi
LIST OF ABBREVIATIONS.....	xxvii
NOTES.....	xxx

TABLE OF CONTENTS

1. Chapter 1	2
1.1. Self-Assembly in Biological Systems	2
1.2. Peptides as Minimal Building Blocks	6
1.3. Types of Peptide Self-Assembled Structures	9
A. Nanotubes	9
B. Fibers.....	12
C. Vesicles	15
1.4. Applications of Self-Assembled Peptides and Pseudopeptides.....	20
A. Drug Delivery and Therapeutics.....	21
B. Tissue Engineering and Regenerative Medicine.....	22
C. Biosensing and Bioimaging	22
D. Catalysis and Enzyme Mimetics.....	22
E. Nanoelectronics and Molecular Devices.....	22
F. Antibacterial and Antiviral Applications	23
G. Vaccine Development and Immunotherapy	23
H. Design Opportunities and Molecular-Level Challenges.....	23
1.5. Conclusion.....	23
1.6. References	25
2. Chapter 2	32
2.1 Introduction	32
2.2 Results and Discussion.....	34
2.3. Conclusions	47
2.4. Methods.....	47
2.4.1. Scanning Electron Microscopy (SEM).....	47
2.4.2. Transmission Electron Microscopy (TEM).....	48

2.4.3. Atomic Force Microscopy (AFM).....	48
2.4.4. Field Emission Scanning Electron Microscopy (FESEM).....	48
2.4.5. NMR titration study.....	48
2.4.6. Confocal Microscopy	48
2.5. General Synthetic Procedure.....	49
2.5.1. Preparation of dipeptide b1	49
2.5.2. Preparation of dipeptide b2	49
2.5.3. Preparation of dipeptide b3	50
2.5.4. Preparation of dipeptide b4	50
2.5.5. Preparation of dipeptide b5	51
2.5.6. Preparation of tripeptide b6	51
2.5.7. Preparation of B1	52
2.5.8. Preparation of B2	53
2.5.9. Preparation of B3	54
2.5.10. Preparation of B4	55
2.5.11. Preparation of B5	55
2.6. References	93
3. Chapter 3	98
3.1. Introduction.....	98
3.2. Results and Discussion.....	101
3.3. Conclusion.....	109
3.4. Experimental Section	109
3.4.1. Scanning Electron Microscopy (SEM).....	109
3.4.2. Atomic Force Microscopy (AFM).....	109
3.4.3. Field Emission Scanning Electron Microscopy (FESEM).....	109
3.4.4. NMR titration study.....	110
3.4.5. Confocal Microscopy	110

3.5. General Synthetic Procedure	110
3.5.1. General Synthetic Procedure of dipeptides c1-c4	110
3.5.2. General Synthetic Procedure of monoureas C1-C4	110
3.5.3. Analytical data of dipeptides c1-c4 and monourea C1-C4	111
3.6. References	141
4. Chapter 4	144
4.1. Introduction	144
4.2. Results and Discussion.....	147
4.3. Conclusion.....	154
4.4. Experimental Section	155
4.4.1. Scanning Electron Microscopy (SEM).....	155
4.4.2. Transmission Electron Microscopy (TEM).....	155
4.4.3. Atomic Force Microscopy (AFM).....	155
4.4.4. Confocal Microscopy	155
4.4.5. NMR titration study.....	155
4.5. General Synthetic Procedure	156
4.5.1. General Synthetic Procedure of dipeptides d2 and d3	156
4.5.2. Synthetic Procedure of Peptide D1	156
4.5.3. General Synthetic Procedure of Peptides D2 and D3	156
4.5.4 Analytical data of dipeptides d2 , d3 and Urea-based peptides D1-D3	157
4.6. References	175
5. Chapter 5	179
5.1. Introduction	179
5.2. Results and Discussion.....	181
5.3. Conclusion.....	190
5.4. Experimental Section	190
5.4.1. NMR titration study.....	190

5.5. General Synthetic Procedure	190
5.5.1. General Synthetic Procedure of dipeptides e1-e4	190
5.5.2. General Synthetic Procedure of monoureas E1-E4	191
5.5.3. Analytical data of dipeptides e1-e4 and monourea E1-E4	191
5.6. References	220

LIST OF FIGURES

Figure 1.1. Different types of hydrophobic interactions; a) hydrogen bonding, b) electrostatic interaction, c) hydrophobic interaction, and d) π - π stacking.	2
Figure 1.2. Collagen Synthesis Mechanism	3
Figure 1.3. Hierarchical formation of quaternary structure of a protein from amino acids.	5
Figure 1.4. Short synthetic peptides self-assembling to well-defined structures like nanotubes, fibers, vesicles and hydrogels.	7
Figure 1.5. Cartoon representation of silver nanowire casting within the nanotube formed by self-assembly of FF dipeptide A1 .	8
Figure 1.6. a) Chemical structure of octapeptide A2 ; b) self-assembly of A2 to form a tubular architecture; c) chemical structures of enantiomers A3 and A4 .	9
Figure 1.7. Chemical structures of nanotube-forming dipeptides A5-A10 and pseudopeptides A11-A12 .	10
Figure 1.8. Chemical structures of triazole-based macrocycle A13 , cystine-based macrocycles A14 and growth hormone-inhibiting peptide Lanreotide; b) Chemical structure and cartoon representation of the stacking of A14 through intermolecular H-bonding, and cartoon.	11
Figure 1.9. Chemical structures of different Fmoc-protected dipeptides A15-A23 .	12
Figure 1.10. Chemical structures of DOPA-based dipeptides A24 and A25 and Amoc-protected dipeptide A26 .	13
Figure 1.11. Chemical structures of Fmoc-protected tripeptide A27 , and tripeptides A28-A31 .	13
Figure 1.12. a) Chemical structures of tripeptides A32 and A33 ; b) cartoon representation of morphological change induced by ultrasound.	14

Figure 1.13. Chemical structures of a) triazole-based macrocycles A34 and A35 , and b) Ser-based pseudopeptides A36-38 .	15
Figure 1.14. Chemical structures of Lys-based PDAs A39-A42 and Phe-based PDA A43 .	16
Figure 1.15. a) Chemical structures of Phg-Phg dipeptide A44 and Cys-Phe-Phe tripeptide A45 , b) Cartoon representation of A46 self-assembling to vesicle-type structures.	16
Figure 1.16. a) Structures of triazolophanes A47 , A48 and A49 , b) Cartoon representation showing vesicle formation.	17
Figure 1.17. Chemical structures of cystine-based peptides A50-A51 , macrocycles A52-A53 and urea-based pseudopeptides A54-A58 .	18
Figure 1.18. a) Chemical structures of linear Arg-Trp based peptide A59 , and its cyclic analogue A60 ; b) chemical structures of self-assembling cyclic peptides A61-A68 .	19
Figure 1.19. Chemical structures of diacetylene-cored pseudopeptides A69-A71 .	20
Figure 1.20. Applications of Self-Assembled Peptides and Pseudopeptides	21
Figure 2.1. Chemical structures of the amino acid-based mono-urea compounds B1-B5 .	32
Figure 2.2. a) Partial ^1H NMR (500 MHz, CD_3CN) spectra of B1 upon the addition of various amounts of $\text{DMSO-}d_6$, b) Influence on NH protons of B1 in CD_3CN by the volume fraction of $\text{DMSO-}d_6$, c) Chemical structure of B1 showing β -turn.	34
Figure 2.3. Possibilities of CO-NH hydrogen bonds in peptide B1 .	36
Figure 2.4. a) Crystal structure of peptide B1 showing turn conformation. Intramolecular edge-to-face π - π interaction is shown as green dotted line, b) CD spectrum of peptide B1 in acetonitrile, c) Space-filling model of aromatic rings showing Phe-Phe zipper. The zoomed-in part shows the orientation of aromatic rings.	36
Figure 2.5. The infrared (IR) spectra comparison of peptide B1 , B2 and B5 showing stretching frequency of ester carbonyls in B1 and B2 at 1737 cm^{-1} , while that of peptide B5 at 1743 cm^{-1} .	37

Figure 2.6. a) Typical Type I' β -turn (PDB id 1KKO) and b) typical Type I β -turn (PDB id 2BK9). The green ribbon traces the backbone of protein. Overlaid images of c) peptide **B1** over typical Type I' β -turn and d) peptide **B2** placed over typical Type I β -turn. The numbering has been done considering each aromatic unit as one atom. 38

Figure 2.7. a) Partial ^1H NMR (500 MHz, CDCl_3) spectra of **B1** at different concentrations, b) Concentration vs chemical shift plot of **B1** in CDCl_3 . 38

Figure 2.8. Crystal structure of peptide **B1** showing N–H \cdots O hydrogen bonds between Aib amide and urea carbonyls with urea NHs. The distances are 2.2 and 2.3 Å respectively. 39

Figure 2.9. a) Association of peptide **B1** through intermolecular π - π interactions and H-bonding to form the tubular structure, b) Intermolecular hydrogen bonded supramolecular tubular structure of peptide **B1**, with dimensions of the cavity are 5 Å and 14 Å. 39

Figure 2.10. SEM images of **B1** show a) nanotubular assembly (indicated by red arrows), b) intermediate stage of microtubule formation (marked by red arrows) and c) microtube structure. TEM images of **B1** show d) nanotubular assembly (indicated by red arrows), e) microtube structure (indicated by red arrows). AFM image of **B1** shows f) microtubular assembly, g) Schematic representation showing the assembly of compound **B1** forming nanotube which eventually aggregate to form microtube. 40

Figure 2.11. FESEM images of **B1** taken at an angle of 10° from the surface showing the open end of the microtubular assembly. The images reveal that tubular assembly is a) triangular, square, and b) hexagonal in shape. The zoomed images are shown in the insets (red arrow showing triangular tube and yellow arrow showing square-shaped tube); c) FESEM images of **B5** taken at an angle of 10° from the surface showing the open end of the microtubular assembly. 41

Figure 2.12. SEM images of a) **B2**, b) **B4** and c) **B5** showing tubular morphology. The sample were prepared by dissolving 1 mg of respective compounds in 1 mL ACN. 42

Figure 2.13. a) FESEM images of **B2** taken at an angle of 10° from the surface showing the open end of the microtubular assembly. 43

Figure 2.14. a) Single crystal structure of compound **B5**, b) Left-handed helical arrangement of **B5**, c) The left-handed helical arrangement of (I) phenyl ring of phenylene urea, (II)

middle phenyl unit (Phe¹), (III) terminal phenyl unit (Phe²), (IV) overlap of (I), (II) and (III) showing a triple helical arrangement. 44

Figure 2.15. Zoomed-in image of triple helix formed by peptide **B5** showing edge-to-face π - π interaction between the aromatic ring of the urea unit (colored in orange) and the phenyl ring of the second Phe-residue (Phe²) (colored in green). 45

Figure 2.16. The interplanar angle between the aromatic rings of consecutive molecules were found to be 60 °. 46

Figure 2.17. a) UV-visible absorption spectra of **B1** at different concentrations. The inset shows partial absorption spectra indicating absorption at higher wavelengths, b) Fluorescence emission spectra for different concentrations of **B1** upon excitation at 365 nm. 46

Figure 2.18. Confocal images of compound **B1** upon excitation at a) 405 nm, b) 488 nm, and c) 560 nm. 47

Figure 2.19. ¹H NMR (500 MHz, CDCl₃) spectrum of **b1**. 57

Figure 2.20. ¹³C NMR (125 MHz, CDCl₃) spectrum of **b1**. 58

Figure 2.21. ESI-Mass spectrum of **b1**. 59

Figure 2.22. ¹H NMR (500 MHz, CDCl₃) of **b2**. 60

Figure 2.23. ¹³C NMR (100 MHz, CDCl₃) spectrum of **b2**. 61

Figure 2.24. ESI-Mass spectrum of **b2**. 62

Figure 2.25. ¹H NMR (500 MHz, CDCl₃) spectrum of **b3**. 63

Figure 2.26. ¹³C NMR (125 MHz, CDCl₃) spectrum of **b3**. 64

Figure 2.27. ESI-Mass spectrum of **b3**. 65

Figure 2.28. ¹H NMR (500 MHz, CDCl₃) spectrum of **b4**. 66

Figure 2.29. ¹³C NMR (125 MHz, CDCl₃) spectrum of **b4**. 67

Figure 2.30. ESI-Mass spectrum of **b4**. 68

Figure 2.31. ^1H NMR (500 MHz, CDCl_3) spectrum of b5 .	69
Figure 2.32. ^{13}C NMR (100 MHz, CDCl_3) spectrum of b5 .	70
Figure 2.33. ESI-Mass spectrum of b5 .	71
Figure 2.34. ^1H NMR (500 MHz, CDCl_3) spectrum of b6 .	72
Figure 2.35. ^{13}C NMR (125 MHz, CDCl_3) spectrum of b6 .	73
Figure 2.36. ESI-Mass spectrum of b6 .	74
Figure 2.37. ^1H NMR (500 MHz, CD_3CN) spectrum of B1 .	75
Figure 2.38. ^{13}C NMR (125 MHz, $\text{DMSO}-d_6$) spectrum of B1 .	76
Figure 2.39. ESI-Mass spectrum of B1 .	77
Figure 2.40. ^1H NMR (500 MHz, CD_3CN) spectrum of B2 .	78
Figure 2.41. ^{13}C NMR (500 MHz, CDCl_3) spectrum of B2 .	79
Figure 2.42. ESI-Mass spectrum of B2 .	80
Figure 2.43. ^1H NMR (500 MHz, CDCl_3) spectrum of B3 .	81
Figure 2.44. ^{13}C NMR (125 MHz, CDCl_3) spectrum of B3 .	82
Figure 2.45. ESI-Mass spectrum of B3 .	83
Figure 2.46. ^1H NMR (500 MHz, CD_3CN) spectrum of B4 .	84
Figure 2.47. ^{13}C NMR (125 MHz, CD_3CN) spectrum of B4 .	85
Figure 2.48. ESI-Mass spectrum of B4 .	86
Figure 2.49. ^1H NMR (500 MHz, CD_3CN) spectrum of B5 .	87
Figure 2.50. ^{13}C NMR (125 MHz, CDCl_3) spectrum of B5 .	88
Figure 2.51. ESI-Mass spectrum of B5 .	89

Figure 3.1. Chemical structures of peptide-based monourea compounds **C1-C4**. 98

Figure 3.2. a) Partial ^1H NMR (500 MHz, CD_3CN) spectra of **C1** upon the addition of various amounts of $\text{DMSO-}d_6$, b) Change in the chemical shift of NH protons of **C1** with the addition of $\text{DMSO-}d_6$, c) Partial ^1H NMR (400 MHz, CD_3CN) spectra of **C1** at different concentrations, d) Change in the chemical shift of NH protons of **C1** with dilution. 100

Figure 3.3. a) Cartoon representation of **C1** showing three intermolecular H-bonds existing in between two molecules; b) Crystal structure of **C1** showing intermolecular hydrogen bonds. 101

Figure 3.4. a) The left-handed arrangement of phenyl unit of peptide **C1** (I) phenyl ring of phenylene urea motif (in apricot orange), (II) middle Phe phenyl unit (in mint green), (III) overlap of (I) and (II) showing a double helical arrangement, b) Phenyl ring of phenylene urea motif sandwiched between two Leu side-chains revealing an Leu-Phe zipper arrangement. 101

Figure 3.5. Crystal structure of peptide **C1** showing $\text{CH-}\pi$ interaction between Leu side-chain CH and N-terminal phenyl group of two neighbouring molecules. 102

Figure 3.6. Crystal packing of peptide **C1** where the urea phenyl group at the N-terminal is sandwiched between the sidechains of leucine (Leu) residue of two neighbouring molecules, revealing a Leu-Phe zipper arrangement. The distances between the Leu side-chain C-Hs and the phenyl ring involved in the zipper assembly formation are both found to be 3.6 Å. 102

Figure 3.7. a) Left-handed helical arrangement of **C1** and its axial view showing the hexameric arrangement of the bundle interconnected to its surrounding six bundles through the Ile-Phe Zipper; b) Cartoon diagram for the heptameric arrangement; c) Urea with Phe as the first residue next to urea moiety leads to the formation of the 6+1 arrangement which further induces tubular assembly. 103

Figure 3.8. Left-handed helical arrangement of **C2** and its axial view showing the 6+1 arrangement of the bundle interconnected to its surrounding six bundles through the Ile-Phe Zipper. 105

Figure 3.9. a) SEM image of **C1** showing tubular assembly, b) FESEM image of **C1** taken at an angle of 20° from the surface, where the inset is showing the open end of the microtubular

assembly, c) SEM image of **C2** showing tubular assembly, d) FESEM image of **C2** taken at an angle of 20° from the surface, where the inset is showing the open end of the microtubular assembly. 106

Figure 3.10. SEM images of a) **C3** and b) **C4** showing fibrous assembly; c) AFM images of compound **C4** revealing fibrous morphology; d) Confocal image of **C4** upon excitation at 488 nm. 107

Figure 3.11. a) Emission spectra and b) variation in fluorescence intensity at 382 nm for different concentrations of **C4** upon excitation at 335 nm, c) Emission spectra of **C4** with different excitation wavelengths, inset of (c) shows the plot of excitation wavelength vs. emission maximum for **C4**, d) Excitation spectra at different emission wavelengths for **C4**. 108

Figure 3.12. ¹H NMR (500 MHz, CDCl₃) spectrum of **c1**. 115

Figure 3.13. ¹³C NMR (125 MHz, CDCl₃) spectrum of **c1**. 116

Figure 3.14. HRMS of **c1** 117

Figure 3.15. ¹H NMR (500 MHz, CDCl₃) spectrum of **c2**. 118

Figure 3.16. ¹³C NMR (125 MHz, CDCl₃) spectrum of **c2**. 119

Figure 3.17. HRMS of **c2**. 120

Figure 3.18. ¹H NMR (500 MHz, CDCl₃) spectrum of **c3**. 121

Figure 3.19. ¹³C NMR (125 MHz, CDCl₃) spectrum of **c3**. 122

Figure 3.20. HRMS of **c3**. 123

Figure 3.21. ¹H NMR (500 MHz, CDCl₃) spectrum of **c4**. 124

Figure 3.22. ¹³C NMR (125 MHz, CDCl₃) spectrum of **c4**. 125

Figure 3.23. HRMS of **c4**. 126

Figure 3.24. ¹H NMR (500 MHz, CD₃CN) spectrum of **C1**. 127

Figure 3.25. ^{13}C NMR (125 MHz, CD_3CN) spectrum of C1 .	128
Figure 3.26. HRMS of C1 .	129
Figure 3.27. ^1H NMR (500 MHz, CD_3CN) spectrum of C2 .	130
Figure 3.28. ^{13}C NMR (125 MHz, CD_3CN) spectrum of C2 .	131
Figure 3.29. HRMS of C2 .	132
Figure 3.30. ^1H NMR (500 MHz, CD_3CN) spectrum of C3 .	133
Figure 3.31. ^{13}C NMR (125 MHz, CD_3CN) spectrum of C3 .	134
Figure 3.32. HRMS of C3 .	135
Figure 3.33. ^1H NMR (500 MHz, CD_3CN) spectrum of C4 .	136
Figure 3.34. ^{13}C NMR (125 MHz, CDCl_3) spectrum of C4 .	137
Figure 3.35. HRMS of C4 .	138
Figure 4.1. Chemical structure of urea-based peptides D1-D3 .	144
Figure 4.2. Partial ^1H NMR (500 MHz, CDCl_3) spectra of D2 at different concentrations.	146
Figure 4.3. Partial ^1H NMR (400 MHz, CDCl_3) spectra of D2 upon the addition of various amounts of DMSO-d_6 , indicating shifts of NHs.	147
Figure 4.4. SEM images of a) D1 , b) D2 and c) D3 , showing fibrous, toroidal and tubular assembly, respectively.	148
Figure 4.5. a) SEM image of peptide D3 , b) zoomed-in image of a single microtube showing an open end of the tube, c) An SEM image of peptide D2 , illustrating the fusion of the inner cavities of several toroids, culminating in the creation of a larger, shared cavity.	148
Figure 4.6. a) Fusion of synthetic lipid membrane vesicles; b) fusion of vesicles from peptide D2 .	149
Figure 4.7. a) Cartoon representation illustrating the mechanism of toroid from vesicles, which are formed through the self-assembly of peptide D2 ; b) The vesicles fuse to create	

hemitoroids, which then approach each other to form a complete toroid; c) Cartoon representation depicting the fusion of toroids, creating a honeycomb-like structure. Subsequent transformation lead to the formation of larger toroids; d) SEM image showing the fusion of toroid to form a double torus (highlighted in red square), while multiple toroids come together to create a honeycomb-like structure (highlighted in yellow square). 150

Figure 4.8. a) TEM and b) AFM images of peptide **D2**. 151

Figure 4.9. TEM images of peptide **D2** showing intermediate stages of toroid formation. 151

Figure 4.10. a) AFM image of toroid formed from self-assembly of peptide **D2**; b) Height profile diagram of the toroid in Figure a; c) Three-dimensional AFM image of the toroid. 152

Figure 4.11. a) UV-visible absorption spectra of **D2** at different concentrations. The inset shows partial absorption spectra indicating absorption at higher wavelengths, b) Fluorescence emission spectra for different concentrations of **D2** upon excitation at 335 nm. 153

Figure 4.12. Confocal images of compound **D2** upon excitation at a) 405 nm, b) 488 nm, and c) 560 nm; d) optical image of compound **D2**; e) overlaid image of a-d. Confocal images of compound **D1** upon excitation at f) 405 nm, g) 488 nm, and h) 560 nm; i) optical image of compound **D1**; j) overlaid image of f-i. 154

Figure 4.13. ^1H NMR (500 MHz, CDCl_3) of **d2** 160

Figure 4.14. ^{13}C NMR (125 MHz, CDCl_3) of **d2** 161

Figure 4.15. ESI-Mass spectrum of **d2** 162

Figure 4.16. ^1H NMR (500 MHz, CDCl_3) of **d3** 163

Figure 4.17. ^{13}C NMR (100 MHz, CDCl_3) of **d3** 164

Figure 4.18. ESI-Mass spectrum of **d3** 165

Figure 4.19. ^1H NMR (500 MHz, CDCl_3) of Peptide **D1** 166

Figure 4.20. ^{13}C NMR (100 MHz, CDCl_3) of Peptide **D1** 167

Figure 4.21. ESI-Mass spectrum of **D1** 168

Figure 4.22. ^1H NMR (500, CDCl_3) of Peptide D2	169
Figure 4.23. ^1H NMR (100 MHz, CDCl_3) of Peptide D2	170
Figure 4.24. ESI-Mass spectrum of D2	171
Figure 4.25. ^1H NMR (500, CDCl_3) of Peptide D3	172
Figure 4.26. ^1H NMR (100 MHz, CDCl_3) of Peptide D3	173
Figure 4.27. ESI-Mass spectrum of D3	174
Figure 5.1. The <i>trans</i> and <i>cis</i> peptide bonds (a) non-Proline peptide and (b) Proline peptide. The dark green indicates most favorable, while light green is favorable, and red is unfavorable interaction.	179
Figure 5.2. Chemical structures of monourea-based peptides E1-E4 .	180
Figure 5.3. Various possible conformers of phenyl urea derivatives at equilibrium.	181
Figure 5.4. a) Partial ^1H NMR (500 MHz, CDCl_3) spectrum of E1 showing one signal for C^δ protons (in red box), b) Partial ^{13}C NMR (125 MHz, CDCl_3) spectrum of showing a single peak for the C^δ carbon, c) Partial ^1H NMR (500 MHz, CDCl_3) spectra of E1 upon the addition of various amounts of $\text{DMSO}-d_6$, d) Influence on NH protons of E1 in CDCl_3 by the addition of $\text{DMSO}-d_6$.	183
Figure 5.5. Partial NMR spectra of peptides E3 and E4 showing two signals for the C^δ protons indicating the existence of two distinct conformers.	184
Figure 5.6. a) Crystal structure of peptide E2 showing <i>trans</i> -form of the proline peptide, which is being stabilized by the $n \rightarrow \pi^*$ interaction; b) Crystal structure of peptide E2 showing C^γ - <i>exo</i> puckering of the pyrrolidine ring; c) Dihedral angle ζ in <i>trans</i> -proline highlighted in blue; d) Cartoon diagram showing pyramidalization in peptide E2 , which is ideal for the $n \rightarrow \pi^*$ interaction; e) <i>exo</i> and <i>endo</i> pyrrolidine ring puckering of a Pro-residue equilibrating with a <i>trans/cis</i> peptide bond.	185
Figure 5.7. Values of dihedral angles χ_1 - χ_4 of peptide E2 ; a) The intermolecular H-bonding between the amide NH and carbonyl C=O leading to the formation of dimer of peptide E2 ; b)	

Arrangement of the peptide **E2** molecules showing alternate occurrence of phenyl ring (in green) and Ile side chain (in pink); c) The dimers of peptide **E2** interconnected to each other through intermolecular H-bonding between urea NH and amide C=O. 186

Figure 5.8. Value of dihedral angle ζ in peptide **E2**. 186

Figure 5.9. a) Surface overlap diagram of phenyl rings and Ile side chains revealing a Ile-Phe Zipper arrangement in **E2**; b) Interdigitated arrangement of consecutive stacks showing each Ile side chain (in pink) surrounded by three phenyl rings (in green); c) Cartoon diagram of interdigitated arrangement of consecutive stacks, where the Ile side chain (knob) (in pink) occupies the hole formed by three phenyl rings (in green) from three different molecules, revealing a Ile-Phe zipper arrangement; d) Cartoon representation of typical zipper arrangement in coiled-coil peptides. 187

Figure 5.10. Partial ^1H NMR spectrum of **E4** showing major and minor signals with a 4:1 ratio for a) NH_c proton and b) C^δ protons. 188

Figure 5.11. ^1H NMR (500 MHz, CDCl_3) spectrum of **e1**. 195

Figure 5.12. ^{13}C NMR (125 MHz, CDCl_3) spectrum of **e1**. 196

Figure 5.13. ESI-Mass spectrum of **e1**. 197

Figure 5.14. ^1H NMR (500 MHz, CDCl_3) spectrum of **e2**. 198

Figure 5.15. ^{13}C NMR (125 MHz, CDCl_3) spectrum of **e2** 199

Figure 5.16. ESI-Mass spectrum of **e2**. 200

Figure 5.17. ^1H NMR (500 MHz, CDCl_3) spectrum of **e3**. 201

Figure 5.18. ^{13}C NMR (125 MHz, CDCl_3) spectrum of **e3**. 202

Figure 5.19. ESI-Mass spectrum of **e3**. 203

Figure 5.20. ^1H NMR (400 MHz, CDCl_3) spectrum of **e4**. 204

Figure 5.21. ^{13}C NMR (100 MHz, CDCl_3) spectrum of **e4**. 205

Figure 5.22. ESI-Mass spectrum of **e4**. 206

Figure 5.23. ^1H NMR (500 MHz, CDCl_3) spectrum of E1 .	207
Figure 5.24. ^{13}C NMR (125 MHz, CDCl_3) spectrum of E1 .	208
Figure 5.25. ESI-Mass spectrum of E1 .	209
Figure 5.26. ^1H NMR (400 MHz, CDCl_3) spectrum of E2 .	210
Figure 5.27. ^{13}C NMR (100 MHz, CDCl_3) spectrum of E2 .	211
Figure 5.28. ESI-Mass spectrum of E2 .	212
Figure 5.29. ^1H NMR (400 MHz, CDCl_3) spectrum of E3 .	213
Figure 5.30. ^{13}C NMR (100 MHz, CDCl_3) spectrum of E3 .	214
Figure 5.31. ESI-Mass spectrum of E3	215
Figure 5.32. ^1H NMR (400 MHz, CDCl_3) spectrum of E4 .	216
Figure 5.33. ^{13}C NMR (100 MHz, CDCl_3) spectrum of E4 .	217
Figure 5.34. ESI-Mass spectrum of E4 .	218

LIST OF TABLES

Table 2.1. Table showing CSI values of peptide B1 and B2	35
Table 2.2. Selected backbone torsional angles ($^{\circ}$) for peptides B1 , B2 and B5	41
Table 2.3. H-bonding distances (\AA) and angles ($^{\circ}$) present in peptide B1	42
Table 2.4. Morphology of peptides B1-B5	43
Table 2.5. Crystal data and structure refinement for peptide B1 (CCDC 2354491).	87
Table 2.6. Crystal data and structure refinement for peptide B2 (CCDC 2354492).	88
Table 2.7. Crystal data and structure refinement for peptide B3 (CCDC 2354493).	89
Table 3.1. Torsional angles ($^{\circ}$) for C1 and C2	104
Table 3.2. Crystal data and structure refinement for peptide C1 (CCDC 2387525).	136
Table 2.5. Crystal data and structure refinement for peptide C2 (CCDC 2387526).	137
Table 4.1. Different geni and their Euler characteristics	145
Table 5.1. H-bonding distances (\AA) and angles ($^{\circ}$) present in peptide E2	189
Table 5.2. Crystal data and structure refinement for peptide E2 (CCDC 2464886).	219

LIST OF SCHEMES

Scheme 2.1. Synthesis of monoureas B1-B5 .	30
Scheme 3.1. Synthesis of monoureas C1-C4 .	96
Scheme 4.1. Synthesis of urea-based peptides D1-D3 .	142
Scheme 5.1. Synthesis of monoureas E1-E4	178

LIST OF ABBREVIATIONS

%	Percent
δ	Chemical shift
$^{\circ}\text{C}$	Degree celsius
ACN	Acetonitrile
ACQ	Aggregation-Caused Quenching
AFM	Atomic Force Microscopy
AIE	Aggregation-Induced Emission
Amoc	9-anthracenemethoxycarbonyl
Boc	tert-Butyloxycarbonyl
CAC	Critical Aggregation Concentration
CDCl_3	Deuterated chloroform
CD_3CN	Deuterated acetonitrile
CSI	Chemical Shift Index
DCC	Dicyclohexylcarbodiimide
DCM	Dichloromethane

DMF	N, N-dimethylformamide
DMSO	Dimethyl sulfoxide
DNA	Deoxyribonucleic Acid
DOPA	Dihydroxy-L-phenylalanine
ECM	Extracellular Matrix
ee	Enantiomeric Excess
EtOAc	Ethyl Acetate
FET	Field-Effect Transistor
FIB	Focused-Ion Beam
FF	Phe-Phe (Diphenylalanine)
Fmoc	9-fluorenylmethoxycarbonyl
HRMS	High-Resolution Mass Spectrometry
JAK/STAT	Janus Kinase/Signal Transducer and Activator of Transcription
LLPS	Liquid-Liquid Phase Separation
MeOH	Methanol
MP	Melting Point
NaHCO ₃	Sodium Bicarbonate

Na ₂ SO ₄	Sodium Sulphate
NMR	Nuclear Magnetic Resonance
NEt ₃	Triethylamine
NHS	N-Hydroxysuccinimide
PBS	Phosphate Buffered Saline
PDA	Polydiacetylene
Phg	Phenylglycine
REES	Red-Edge Excitation Shift
SEM	Scanning Electron Microscopy
SH2	Src Homology 2
SPPS	Solid Phase Peptide Synthesis
TEM	Transmission Electron Microscopy
TLC	Thin Layer Chromatography
TFA	Trifluoroacetic acid
Trpzip	Tryptophan zipper
UV	Ultraviolet

NOTES

1. All amino acids used in syntheses were of L-configuration, unless stated otherwise, and were purchased from SRL India. Unless otherwise stated, the standard single/triple letter codes are used to represent amino acids.
2. All commercial chemicals and reagents used in chemical syntheses were purchased from Sigma-Aldrich or SRL India unless otherwise stated, and used as received without any further purification.
3. All the solvents employed in the reactions were distilled/dried by standard protocols prior to use.
4. All air sensitive reactions were carried out in oven dried glassware under an inert atmosphere of argon.
5. All the reactions were monitored by silica gel thin layer chromatography (TLC), wherever possible.
6. All the synthesized compounds were purified by silica gel (100-200 mesh) column chromatography. The slurry was generally made in chloroform, DCM and/or MeOH.
7. The characterization of synthesized compounds was done by ^1H NMR, ^{13}C NMR, IR and High-Resolution Mass Spectrometry (HRMS).
8. ^1H and ^{13}C NMR spectra were recorded on a Bruker-DPX-400/500 MHz spectrometer and the chemical shifts are reported downfield relative to tetramethylsilane (TMS). ^1H NMR data are reported as br (broad), s (singlet), d (doublet), q (quartet), t (triplet), dd (doublet of doublet) and m (multiplet). ^1H NMR coupling constants are reported in Hz.
9. High resolution mass spectra (HRMS) were recorded in Bruker MicrO-TOF-QII model using Electrospray Ionization (ESI) technique.
10. IR spectra were recorded on Agilent-Cary 660 Series FTIR spectrometer/Nicolet, Protégé 460 spectrometer as KBr Pellets.
11. Melting points were recorded on a Fisher-Scientific melting point apparatus.